

Short communication

# Physicochemical characterization and adsorptive properties of some Moroccan clay minerals extruded as lab-scale monoliths

Sanae Harti<sup>a</sup>, Gustavo Cifredo<sup>b</sup>, José Manuel Gatica<sup>b</sup>, Hilario Vidal<sup>b</sup>, Tarik Chafik<sup>a,\*</sup>

<sup>a</sup> *Laboratoire de Génie Chimique et Valorisation des Ressources, Faculté des Sciences et Techniques de Tanger, Université Abdelmalek Essaadi, B.P. 416 Tangier, Morocco*

<sup>b</sup> *Departamento C.M., I.M. y Química Inorgánica, Universidad de Cádiz, Puerto Real 11510, Spain*

Received 22 March 2006; received in revised form 2 October 2006; accepted 12 October 2006

Available online 1 December 2006

## Abstract

Textural, structural and adsorptive properties of some Moroccan clays were investigated. The minerals were used as raw material for extrusion of honeycomb monoliths. Adsorption and desorption tests were performed with selected model pollutants such as volatile organic compounds (VOCs). The clays have been chosen, apart from their abundance and price, on the basis of successful extrusion as integral lab-scale honeycomb monoliths. The obtained monoliths have been subjected to measurements of the mechanical strength.

© 2006 Elsevier B.V. All rights reserved.

*Keywords:* Clays; Honeycomb monoliths; VOCs; Adsorption

## 1. Introduction

The physicochemical properties of clay minerals and their abundance associated with their relatively low cost justify the numerous traditional uses in ceramics, paper, paint, plastics, drilling fluids, chemical carriers, liquid barriers, decolorization, and even other more advanced applications such as in catalysis (Ciullo, 1996). Improvement of mining and processing techniques will lead to further growth of traditional applications and to development of innovative products involving clay minerals (Murray, 2000). In this sense, the present paper introduces some Moroccan clay as raw materials for extrusion of honeycomb monoliths disposing of an adequate combination of physicochemical and mechanical properties.

Honeycomb monoliths have the advantage of presenting low pressure drop that allows working with high flow rates, which is more suitable for environmental applications as adsorbent material and/or catalyst support (Heck et al., 2002). The extrusion process requires pastes of adequate plasticity in order to permit immediate conformation in a rigid monolithic structure (Avila et al., 2005). This is sometimes a tedious task requiring great effort, particularly, when new material is used. In this study, we use the methodology based on extension of procedures usually employed to extrude ceramics (Gatica et al., 2004). The textural and morphological properties (particle size, shape and distribution, porosity, surface area) have been investigated using powdered samples of the clays that have been successfully extruded. For this purpose SEM and N<sub>2</sub> gas adsorption/desorption techniques have been applied. The compositions were determined by EDS, structural properties by XRD and FTIR spectroscopy, and thermal stability by TGA and TPD-MS. The obtained

\* Corresponding author. Tel.: +212 39393954/55; fax: +212 39 39 39 53.

E-mail addresses: [tchafik@yahoo.com](mailto:tchafik@yahoo.com), [chafik@fstt.ac.ma](mailto:chafik@fstt.ac.ma) (T. Chafik).

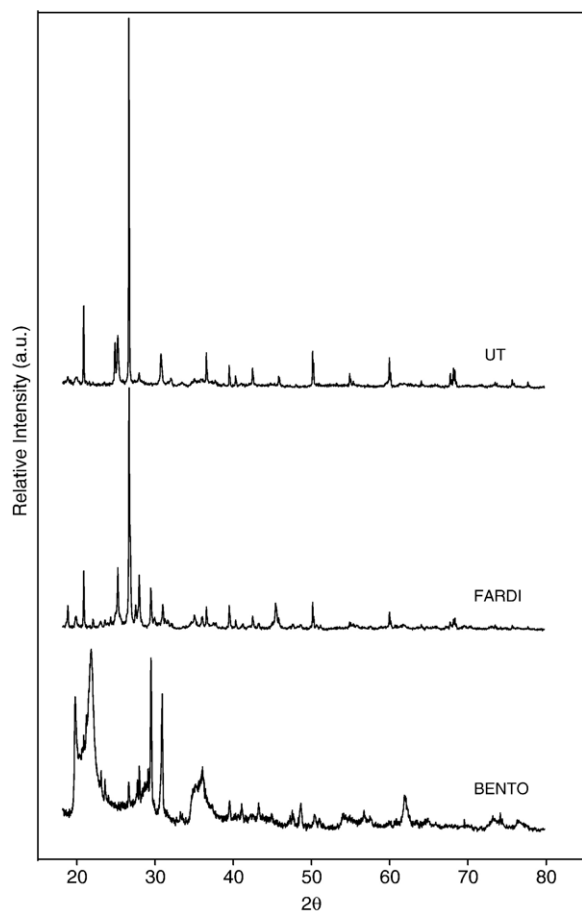


Fig. 1. X-ray diffractograms of the clays.

results have been correlated with adsorption and desorption data of a model volatile organic pollutant (VOC) of xylene type. The latter experiments were performed under dynamic conditions according to a methodology reported elsewhere (Zaitan and Chafik, 2005).

The present study could be a starting point for further development of innovative materials for applications in efficient and economical environmental engineering control technologies. The final objective is to contribute to local sustainable development.

## 2. Materials and methods

### 2.1. Materials

The tested clays samples were obtained from different deposits located in the north of Morocco. The so-called UT is original from Tangier, the BENTO sample proceeds from the Nador area and the clay denoted FARDI comes from the area of Tetuan. All the samples were first crushed and passed through a 180  $\mu\text{m}$  sieve before any use.

### 2.2. Characterization techniques

Textural characterization of the clays has been carried out by measuring the adsorption/desorption of  $\text{N}_2$  at 196  $^\circ\text{C}$ , using a Micromeritics ASAP 2020. The samples were heated under high vacuum at 200  $^\circ\text{C}$  for 30 min. TGA was carried out under air with a Shimadzu TGA-50 thermobalance using 20 mg samples and a heating rate of 10  $^\circ\text{C}/\text{min}$ . Complementary Temperature Programmed Desorption (TPD) experiments were performed using a Pfeiffer Vacuum Balzers mass spectrometer (MS), model QMS 200, operated with Quadstar 32-Bit software for data acquisition and processing. The experiments were carried out with 200 mg samples heated at a 10  $^\circ\text{C}/\text{min}$  rate starting from room temperature up to 950  $^\circ\text{C}$ , under He flow of 60  $\text{cm}^3/\text{min}$ . SEM images and EDS data were obtained with a QUANTA-200 Scanning Electron Microscope (Philips) equipped with a Phoenix Microanalysis System using a nominal resolution of 3 nm. XRD was performed at room temperature using a Bruker D8-500 powder diffractometer operating with Cu  $\text{K}\alpha$  radiation. The  $2\theta$  angle ranged from 14 $^\circ$  to 65 $^\circ$  with a step of 0.03 $^\circ$  and a counting time of 5 s, from 65 $^\circ$  to 105 $^\circ$  with a step of 0.05 $^\circ$  and a counting time of 7 s, and from 105 $^\circ$  to 145 $^\circ$  with a step of 0.07 $^\circ$  and a counting time of 9.5 s. Rietveld analysis was performed using the Fullproof program (Rodríguez-Carvajal, 1993). A conventional IR quartz cell equipped with  $\text{CaF}_2$  windows was used to carry out treatment of self-supported sample wafers as well as spectra measurements. After evacuation under high vacuum at 200  $^\circ\text{C}$  for 30 min, the spectra were recorded in absorbance mode, by performing 100 scans from 4000 to 400  $\text{cm}^{-1}$  with a resolution of 4  $\text{cm}^{-1}$ , using a VERTEX 70 FTIR instrument operated with OPUS software.

The performances with respect to pollutant adsorption/desorption were measured under dynamic conditions using a homemade apparatus as previously reported (Zaitan and Chafik, 2005). The gas mixture of *o*-xylene and  $\text{N}_2$  was prepared by mean of a saturator associated with a condenser that was immersed in a thermostatically controlled bath to keep the temperature at 10 $\pm$

Table 1

Mineralogy information of the studied clays according to X-ray Diffraction analysis

Material	Mineralogical composition
BENTO <sup>a</sup>	Opal, montmorillonite, kaolinite, muscovite, topaz, rutile, calcite, dolomite
FARDI <sup>b</sup>	Quartz (01-087-2096), muscovite (00-007-0042), clinocllore (00-029-0701), anorthite (01-078-2330), sanidine (01-087-0684), calcite (01-089-1304)
UT <sup>b</sup>	Quartz (01-087-2096), clinocllore (00-029-0701), pennine (01-083-1365), sepiolite (01-075-1597), ankerite (00-041-0586)

<sup>a</sup> Rietveld analysis was performed using the crystallographic information available in literature for each phase except in the case of opal for which simulation was carried out from values of tetragonal  $\alpha$ -cristobalite slightly modified according to its intermediate structure between those corresponding to cristobalite and tridymite.

<sup>b</sup> Phase identification was carried out according to the ICDD database. The corresponding PDF code is indicated into brackets.

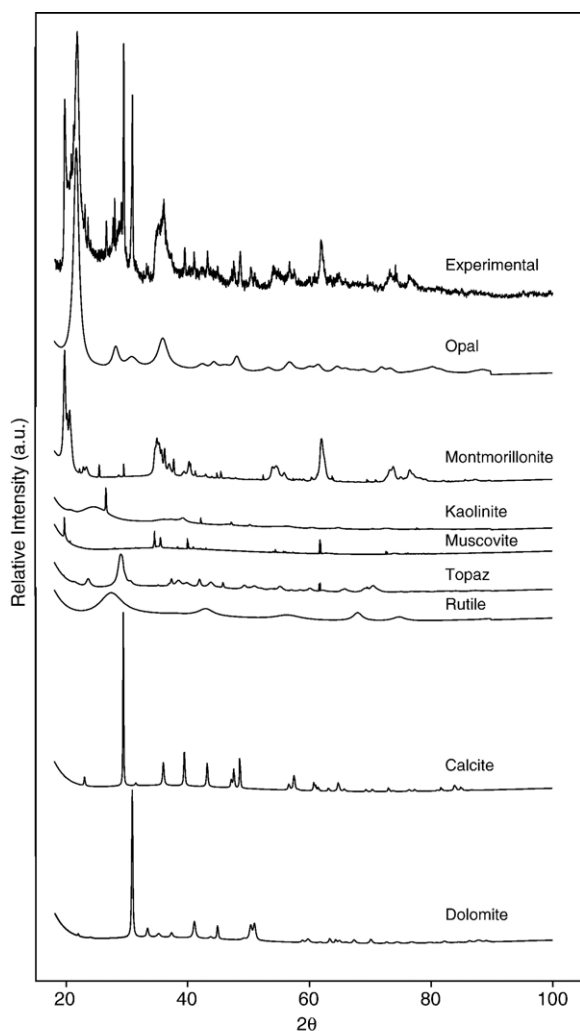


Fig. 2. X-ray diffractogram of BENTO clay and the associated phases deduced from Rietveld analysis.

0.5 °C. These conditions lead to a mixture containing 3600 ppm of xylene in N<sub>2</sub> which has been used with a total flow of 100 cm<sup>3</sup>/min. The adsorption tests were carried out at 27 °C with a quartz reactor using 1 g of the powdered clay which has been subjected to an in situ treatment in N<sub>2</sub> flow (100 cm<sup>3</sup>/min) at 210 °C for 30 min. After the sample saturation, the gas mixture was replaced by pure nitrogen flow (100 cm<sup>3</sup>/min) to proceed with isothermal desorption at 27 °C until the *o*-xylene concentration reached zero. This step was followed by a temperature programmed desorption (TPD) experiment using a heating rate of 5 °C/min. The gas composition at the outlet of the reactor was measured with a FTIR spectrometer (Jasco 410, resolution 4 cm<sup>-1</sup>), using a Pyrex gas cell equipped with CaF<sub>2</sub> windows. Quantitative FTIR data were obtained by integrating the characteristic *o*-xylene FTIR bands located between 2600 and 3200 cm<sup>-1</sup>, on the basis of prior calibration performed with mixtures of known *o*-xylene concentration.

Finally, extrudability assays were achieved following the methodology previously developed (Gatica et al., 2004). It is

necessary to know the plasticity parameters of the paste to be extruded. The liquid limit LL corresponds to the amount of water when the clay loses its fluidity (standard procedure UNE 103-103-94). The plasticity index PI is given by LL-PL, where the plastic limit PL indicates the water content when the clay is moldable (standard procedure UNE 103-104-93). In the present study, a machine was used for extrusion of dough to elaborate honeycomb square section monoliths with a cell density of four cells/cm<sup>2</sup>, in 2 × 2 or 4 × 4 configurations, and a wall thickness of 1.3 mm. Depending on the clay material, different additives besides water were used to allow extrusion, such as a natural coal kindly supplied by the National Institute of Carbon of Spain, aluminum phosphate hydrate (dissolved in *o*-phosphoric acid) from Riedel-de-Haën, pure methylcellulose provided by Panreac S.A. and pure aluminum stearate from Fluka.

After extrusion, axial crushing strength of the monoliths was measured employing a Shimadzu AG-IS Universal Machine for mechanical assays working at a maximum pressure of 100 kN, according to the standard procedure UNE-EN ISO 604.

### 3. Results and discussion

#### 3.1. Structure, composition and morphology

The mineralogical composition was determined from the X-ray diffraction patterns (Fig. 1) on the basis of the International Center for Diffraction Data (ICDD) data

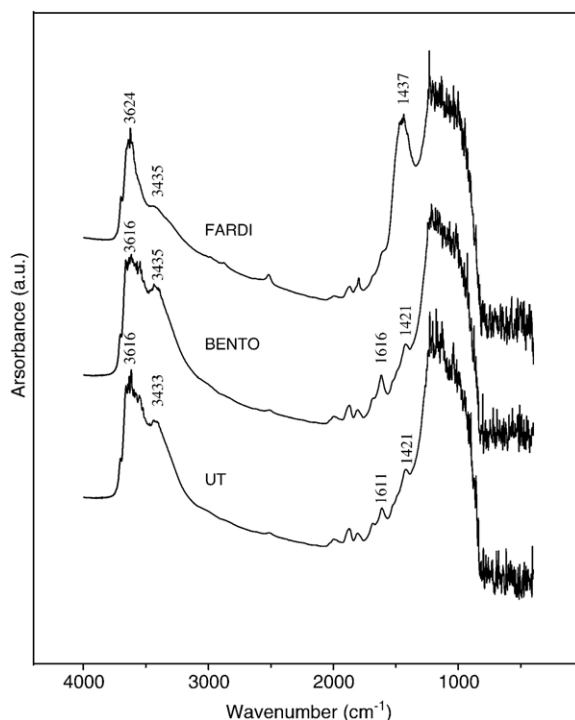


Fig. 3. FTIR spectra of the studied clays recorded after evacuation for 30 min under high vacuum at 200 °C.

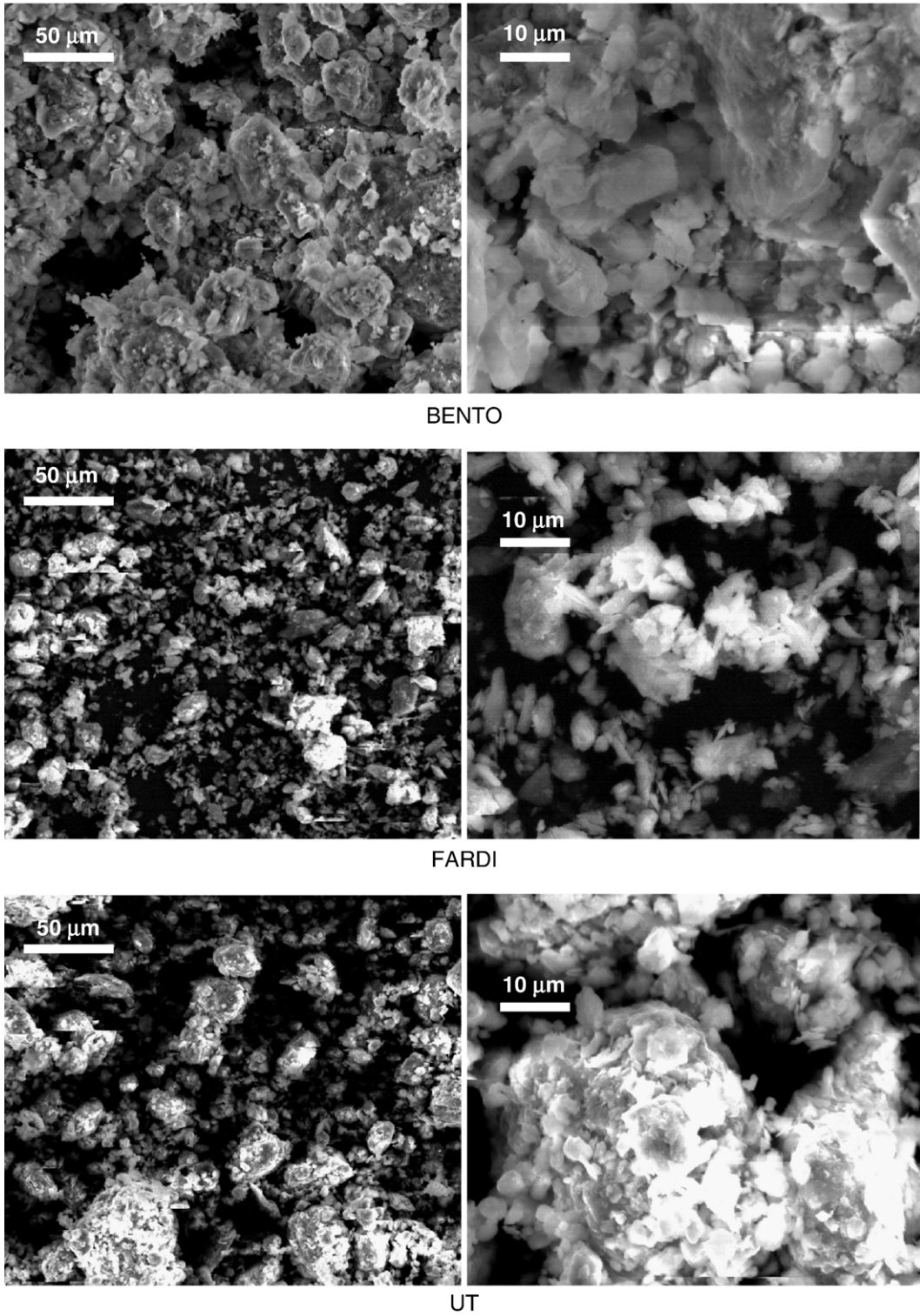


Fig. 4. Scanning electron micrographs of the clays at different magnifications.

Table 2  
EDS elemental analysis of the clays (wt. %)

Clay	O	Si	Al	C	Na	K	Mg	Ca	Fe	Ti	Cl
BENTO	48.4	32.8	7.0	–	0.8	0.5	1.9	4.9	3.4	–	0.3
FARDI	48.9	20.8	8.9	8.3	1.2	2.4	2.1	2.7	4.7	–	–
UT	36.6	23.3	8.3	2.0	–	2.5	1.6	1.4	22.4	1.9	–

base (Table 1). The studied samples contain different minerals such as montmorillonites and micas, hornblende, feldspars, chlorites, carbonates, and oxides. In the particular case of BENTO sample, an additional Rietveld study was performed (Fig. 2) due to its more complex mineralogical composition.

The spectra presented in Fig. 3 show an interesting IR band located at  $1437\text{ cm}^{-1}$  which is much more intense for FARDI than BENTO and UT. According to Nakamoto (1977) this feature corresponds to carbonates which are apparently related with the presence of calcite in agreement with our XRD data. The presence of this phase might be more pronounced for FARDI sample than the calcite and dolomite contained in BENTO or ankerite in UT samples (Table 1). Similar observations have been, therefore, reported by Alami et al. (1998). The IR bands located at  $3620$  and  $3435\text{ cm}^{-1}$  (shoulder) for the spectra recorded with the three samples, correspond, respectively to OH stretching and interlayer water vibrations (Christidis et al., 1997).

SEM micrographs (Fig. 4) show that BENTO presents typical smectite flakes, also previously reported for bentonite from Greece (Christidis et al., 1997). UT and FARDI display different agglomerates of particles with heterogeneous size. Observation at higher magnification also denotes that particles observed for BENTO sample, although presenting irregular forms, are more flatted in some areas, generally contained in bentonite type clay. The results of EDS complementary microanalysis (Table 2) indicate the existence of elements usually present in clay minerals. The higher Si/Al ratio in BENTO and the higher iron content in UT should be mentioned. This is in good agreement with the empirical phase composition revealed by XRD analysis, particularly the presence of montmorillonite and iron-containing phases such as ankerite and pennine (Table 1). Although the carbon analysis is close to the detection limit of EDS technique, the obtained value is clearly higher for FARDI supporting the higher carbonate content illustrated by our FTIR result.

### 3.2. Thermal analysis

The thermal analysis of the studied clays presents three or four main stages of weight loss during the

heating process (Fig. 5). The first loss occurs between room temperature and  $\sim 200\text{ }^{\circ}\text{C}$ , with a maximum rate of weight loss around  $90\text{ }^{\circ}\text{C}$  for BENTO sample. The second loss is not so well defined and extends up to

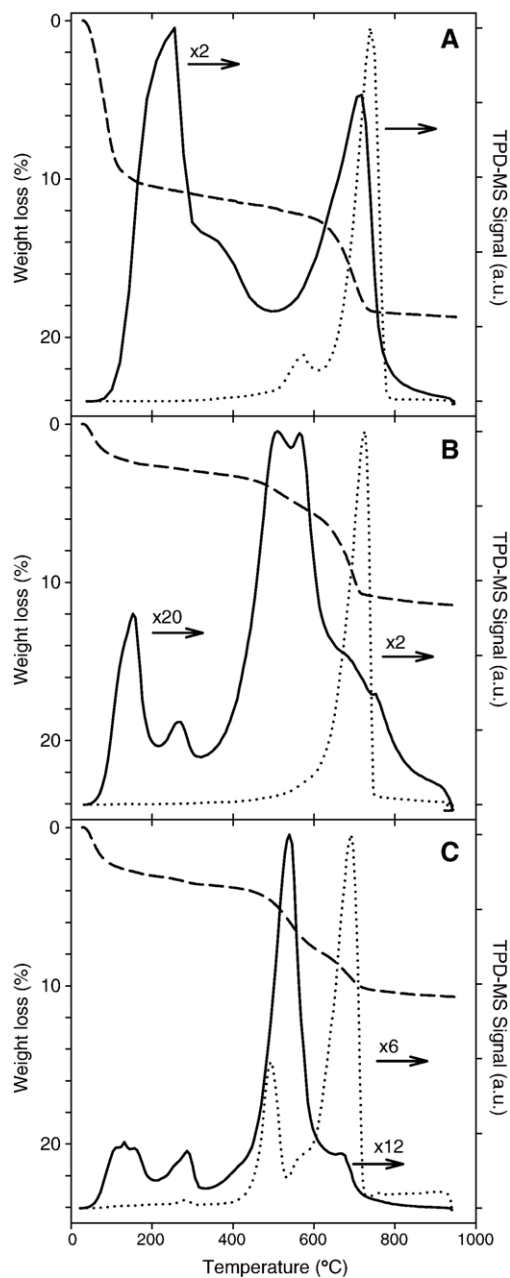


Fig. 5. Thermogravimetric analysis (dashed line) and TPD-MS diagrams obtained with the studied clays: A) BENTO, B) FARDI and C) UT.  $\text{H}_2\text{O}$  ( $m/e$ : 18, solid line) and  $\text{CO}_2$  ( $m/e$ : 44, dotted line) were the only gaseous products detected. The TPD diagrams have been corrected considering the mass spectrometer sensitivity to the different species analyzed and have been normalized for comparative purposes (notice magnification factors).

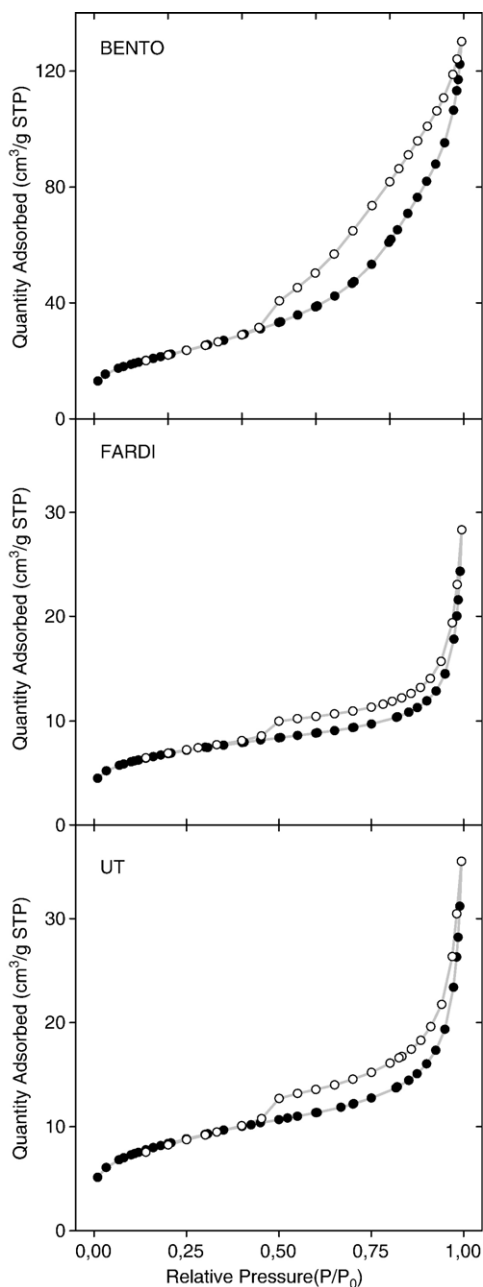


Fig. 6. N<sub>2</sub> adsorption/desorption isotherms. Adsorption (●) and desorption (○) branches.

450 °C for UT and FARDI samples and up to 600 °C for BENTO. In UT and FARDI a third stage extends from 450 to 600 °C. Finally, the last stage in all the samples starts at 600 °C approximately extending up to ~725 °C and centered at 690 °C in the particular case of BENTO sample. It is additionally remarkable that the BENTO clay exhibits the highest weight loss corresponding to roughly 11% of the sample mass during the first stage.

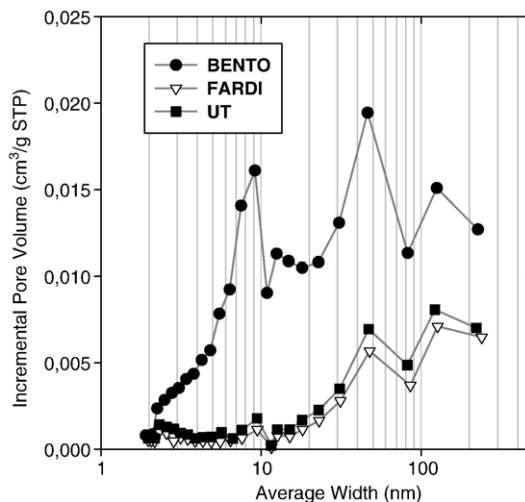


Fig. 7. Pore size distribution of the clays as determined by the BJH method.

Fig. 5 includes also the profiles of  $m/e=18$  and  $m/e=44$  signals, corresponding to water and carbon dioxide (the only gaseous products detected) evolved during TPD-MS experiments carried out with the same heating rate than TG analysis. Accordingly, the weight loss observed at lower temperatures is associated with the elimination of water vapor typically retained by the surface of a porous material. Since this first weight loss is more pronounced for BENTO, it could be considered as first indication of higher surface area if compared with other samples. The TPD signals associated with the second loss might be related with water released either by hardly accessible pores and/or solid dehydroxylation and CO<sub>2</sub> production resulting from carbonate decomposition. This explanation is justified by the fact that water and CO<sub>2</sub> signals present different peak maxima (Fig. 5). The same phenomenon is also exhibited by TPD result obtained at temperature range higher than 600 °C which is, apparently, associated with further dehydroxylation (Augustine, 1996) as well as carbonate decomposition and CO<sub>2</sub> elimination. This interpretation is supported by

Table 3

Textural properties of the powdered and extruded (into brackets) samples

Sample	Pore volume (cm <sup>3</sup> /g)		
	S <sub>BET</sub> (m <sup>2</sup> /g)	Micropores *	Total **
BENTO	79 (80)	0.002 (0.015)	0.205 (0.115)
FARDI	23 (12)	0.003 (0.002)	0.039 (0.037)
UT	29 (28)	0.002 (0.002)	0.054 (0.060)

\* Micropores estimation according to t-plot method.

\*\* Total pore volume calculated following BJH adsorption cumulative pores volume method.

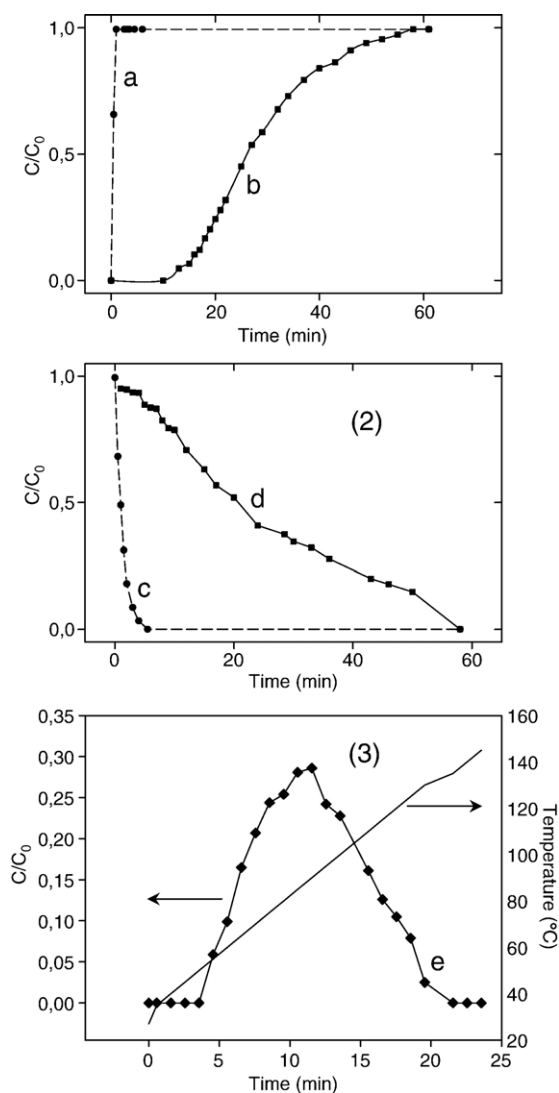


Fig. 8. *O*-xylene adsorption/desorption on BENTO. Graph 1: a) blank response, b) adsorption experiment at 27 °C with *o*-xylene (3600 ppm)/ N<sub>2</sub> mixture; Graph 2: c) reactor by-pass curve, and d) isothermal desorption at 27 °C under pure N<sub>2</sub> flow after the adsorption step; Graph 3: e) TPD after the isothermal desorption step.

our XRD and FTIR analyses revealing the presence of different carbonate types in the studied samples.

On the basis of our analysis, heating under inert gas flow at 200 °C can be enough to clean the clay mineral surface without changing structure and should be carried out prior to any adsorption investigations.

### 3.3. Textural study

The N<sub>2</sub> adsorption/desorption isotherms obtained with the tested raw clays (Fig. 6) are likely of type IV,

Table 4  
*O*-xylene adsorption/desorption data obtained with the studied clays

Clay	Total adsorption capacity at 27 °C (μmol/g)	Reversible amount (μmol/g) *	T <sub>m</sub> (°C) **
BENTO	416	365	95
FARDI	111	90	55
UT	129	76	65

\* As determined by means of isothermal desorption at 27 °C.

\*\* Temperature of peak maximum of TPD profiles.

characteristic of relatively large pores (Gregg and Sing, 1982). Besides clearly higher amounts of nitrogen adsorbed, the isotherm of BENTO sample presents a significantly different hysteresis loop denoting the existence of a more complex porosity. This is confirmed by comparison of different pore size distributions obtained by means of BJH analysis (Fig. 7). BENTO sample presents wider pore sizes in the mesopores range with a significant contribution of pores around 9 nm of width, which is not the case of the other two clays. The data concerning BET surfaces and porosities collected in Table 3 show that micropores are negligible in all tested clays. The highest values of the specific surface area and the total pore volume are obtained with BENTO sample.

### 3.4. Adsorptive behavior

Fig. 8 represents the *o*-xylene breakthrough, isothermal desorption and the TPD curves with BENTO sample. The adsorbed and desorbed amounts of xylene (Table 4) were calculated by integration of these curves

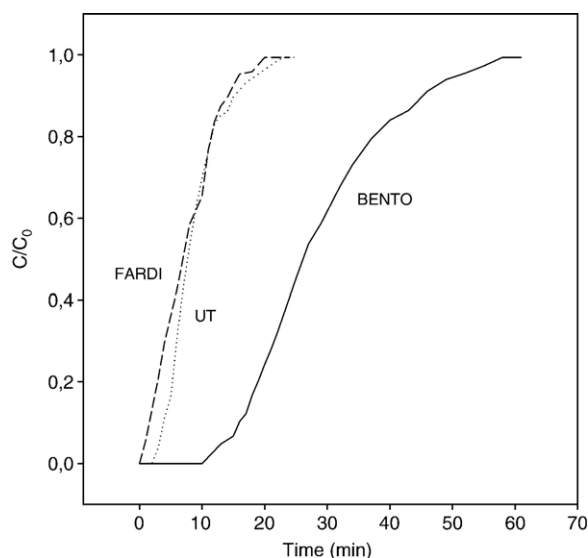


Fig. 9. Comparison between the breakthrough curves corresponding to the *o*-xylene adsorption tests.

Table 5  
Doughs optimal composition and plasticity parameters for monoliths preparation

Clay	Additives (wt. %) <sup>1</sup>				Plasticity parameters	
	Natural coal	AP <sup>a</sup>	Methyl cellulose	Aluminium stearate	LL (%) <sup>b</sup>	PI (%) <sup>c</sup>
BENTO	29.1	2.9	–	–	38.2	36.5
FARDI	–	0.5	1	0.2	48.4	26.1
UT	19.9	–	–	0.5	55	37

<sup>1</sup> Weight percentages referred to the paste excluding water.

<sup>a</sup> Aluminium phosphate hydrate dissolved in *o*-phosphoric acid.

<sup>b</sup> Liquid limit.

<sup>c</sup> Plasticity index.

following a recently reported procedure (Zaitan and Chafik, 2005). The obtained data summarized in Table 4 indicate that BENTO sample exhibits an adsorption capacity comparable to activated carbon adsorbents (Wang et al., 2004; Gatica et al., 2006). Hence, the adsorption capacities follow the trend shown by the specific surface area and total porosity: BENTO  $\gg$  UT > FARDI. However, correlation of adsorption capacity values with textural properties (BET surface area and porosity) is not so evident if aspects related to reversible and irreversible adsorption are considered. The reversible fraction (Table 4) is higher than 80% for FARDI and BENTO and 59% for UT. According to Fig. 6 the shape of the hysteresis loops for FARDI and UT are similar but different from those of BENTO so that the high amount of irreversibly adsorbed xylene by UT cannot be related to the textural properties. According to Tables 1 and 2, the clays reveal significant differences in their composition, both from elemental and mineralogical point of view. Further research is needed to investigate the interaction strengths of *o*-xylene with these samples. Fig. 9 shows a superposition of breakthrough curves obtained during *o*-xylene isothermal adsorption experiments. The better adsorptive performance of BENTO is evident and not only exhibits a larger total adsorption during the first minutes but also requires about 60 min to saturate a sample of 1 g, while around 20 min were enough for the other clays under the experimental conditions here investigated.

Table 4 also includes the temperature of the maximum desorption rate ( $T_m$ ) observed during the TPD experiments. Even if there is a slight difference between the  $T_m$  values this temperature does not exceed 100 °C. This performance is much better than the one exhibited by carbon-based honeycomb monoliths (materials conventionally used for this kind of application) for which temperatures as high as 300 °C were necessary to

achieve total desorption of *o*-xylene adsorbed under similar experimental conditions (Gatica et al., 2006). This result is significant in terms of adsorbent regeneration because all the studied clays present an economical advantage with respect to easier pollutant recovery after saturation. Summarizing, BENTO not only presents a higher capacity to adsorb *o*-xylene but also shows longer adsorption efficiency with time and easy regeneration. These aspects are of interest for consideration under industrial operating conditions.

### 3.5. From powders to monoliths

Taking into account the promising properties exhibited by the studied clays, especially BENTO sample, and considering their low cost, extrusion tests were performed so as to elaborate honeycomb monoliths, which is sometimes, more suitable shape for environmental technology (Heck et al., 2002). The method consists on using a mixture of different chemical reactants added to the clay in order to facilitate extrusion. Following this step, plastic properties are measured, such as liquid limit (LL) and plasticity index (PI). According to the Casagrande's technique (Gippini, 1979) on which this method is based, extrusion will be successfully achieved if a dough exhibits simultaneously values of LL and PI located within  $40\% < LL < 60\%$  and  $10\% < PI < 30\%$ . Table 5 summarizes the optimal composition of doughs as well as the plasticity parameters obtained following sequence of tests carried out up to fulfill extrusion requirements. After obtaining the appropriate composition of each paste, extrusion tests were successfully

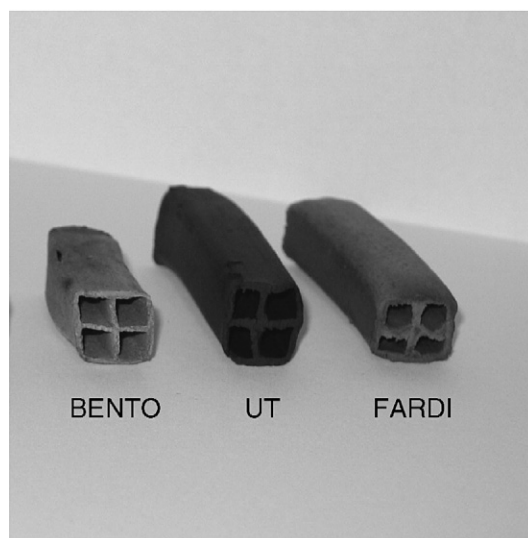


Fig. 10. The obtained clay monoliths in 2 × 2 configuration.

performed in all cases. For BENTO and UT some pastes were extruded in spite of having LL and PI parameters slightly out of the extrudability limits. The results here presented show the validity of the method which had been originally developed for ceramics and successfully adapted, also, to carbonaceous materials (Gatica et al., 2004; Rodríguez-Izquierdo et al., 2005). The obtained honeycomb monoliths resulting from the studied clay are shown in Fig. 10.

Further TPO experiments (results not shown) have been carried out with the extruded monoliths in order to check out the experimental conditions needed for complete removal of the additives. It was found that heating at 400 °C under air flow (120 cc/min) for 2 h was appropriate and enough to achieve additive elimination. So far, there are no significant differences, above 400 °C, between TPO and TPD (Fig. 5) data, obtained respectively with samples of extruded and powder forms. Additionally, the textural data given in Table 3 allow us to state that the treatment leading to additives removal from the monoliths does not lead to major changes in the textural properties as compared to those of raw clays.

Measurement of the axial crushing strength of the monoliths reveals relative good mechanical properties. For BENTO and UT mechanical resistance against breaking under pressure along the channel direction was about 2.7 MPa and 1.9 MPa respectively, but a significantly higher value was measured for FARDI (7.1 MPa). These values are certainly lower than those published for monoliths based on pillared clay materials but prepared in the form of cylindrical extrudates (Mohino et al., 2005). However, the comparison is more favorable when honeycomb monoliths are taken as references. For instance, our results are just slightly lower than those reported for monoliths prepared from ceramic composites (Yates et al., 2000) or for carbon coated cordierite monoliths (Valdés-Solís et al., 2001), and similar (Vergunst et al., 2001) or even better than those reported for integral-type carbon monoliths (Gatica et al., 2006).

#### 4. Conclusions

Three clays from the north of Morocco were investigated at laboratory scale so as to assess their potential use as monoliths for environmental applications. Among the studied sample, the bentonite type clay, BENTO, exhibited higher adsorption capacity for *o*-xylene, which remained efficient with time and required heating at lower temperature to recover its initial adsorptive performances.

Investigation of textural properties and characterization study using SEM-EDS, X-ray diffraction and FTIR spectroscopy were used to understand the differences in the adsorption capacity of the clays.

Extrapolation of methodology initially employed with ceramics and previously applied to carbon-based materials was successfully used to extrude honeycomb type monoliths. Mechanical studies demonstrated that the monoliths exhibit acceptable strengths.

The above results could be a starting point for further development of filters and catalysts using relatively low cost and abundant raw materials such as natural clays with a target of valorisation that may give added value in a context of local sustainable development.

#### Acknowledgements

This work has been funded by the AM17/04 Project of the Junta de Andalucía (Spain). The authors thank Prof. A. Benmoussa from Geology Department at Sciences Faculty of Tetuan for providing the clay samples, Dr. H. Zaitan from Abdelmalek Essaadi University for the VOC adsorption measurements and D. Sanchez from the LABCYP group of Cadiz University for helping with the mechanical resistance measurements. They also acknowledge the Central Service of Science and Technology of the University of Cadiz for using its SEM and XRD facilities.

#### References

- Alami, A., Boulmane, M., Hajjaji, M., Kacim, S., 1998. Chemicomineralogical study of a moroccan clay. *Annales de Chimie, Science des Matériaux* 23, 173–176.
- Augustine, R.L., 1996. *Heterogeneous catalysts for the synthetic chemist*. Marcel Dekker Inc., New York.
- Avila, P., Montes, M., Miró, E., 2005. Monolithic reactors for environmental applications. A review on preparation technologies. *Chemical Engineering Journal* 109, 11–36.
- Christidis, G.E., Scott, P.W., Dunham, A.C., 1997. Acid activation and bleaching capacity of bentonites from the islands of Milos and Chios, Aegean, Greece. *Applied Clay Science* 12, 329–347.
- Ciullo, P.A., 1996. *Industrial Minerals and their uses: A handbook and formulary*. William Andrew Inc., New Jersey.
- Gatica, J.M., Rodríguez-Izquierdo, J.M., Sánchez, D., Ania, C.O., Parra, J.B., Vidal, H., 2004. Extension of preparation methods employed with ceramic materials to carbon honeycomb monoliths. *Carbon* 42, 3251–3254.
- Gatica, J.M., Rodríguez-Izquierdo, J.M., Sánchez, D., Chafik, T., Harti, S., Zaitan, H., Vidal, H., 2006. Originally prepared carbon-based honeycomb monoliths with potential application as VOCs adsorbents. *Comptes Rendus Chimie* 9, 1215–1220.
- Gippini, E., 1979. *Pastas Cerámicas*. Sociedad Española de Cerámica, Madrid.
- Gregg, S.J., Sing, K.S.W., 1982. *Adsorption surface area and porosity*. Academic Press, London.

- Heck, R.M., Farrauto, R.J., Gulati, S.T., 2002. *Catalytic Air Pollution Control: Commercial Technology*. John Wiley, New York.
- Mohino, F., Martín, A.B., Salerno, P., Bahamonde, A., Mendioroz, S., 2005. High surface area monoliths based on pillared clay minerals as carriers for catalytic processes. *Applied Clay Science* 29, 125–136.
- Murray, H., 2000. Traditional and new applications for kaolin, smectite, and palygorskite: a general overview. *Applied Clay Science* 17, 207–221.
- Nakamoto, K., 1977. *Infrared and Raman Spectra of Inorganic Coordination Compounds*, 3rd edn. John Wiley and Sons, New York.
- Rodríguez-Carvajal, J.J., 1993. Recent advances in magnetic structure determination by neutron powder diffraction. *Physica. B, Condensed Matter* 192, 55–69.
- Rodríguez-Izquierdo, J.M., Vidal, H., Gatica, J.M., Sánchez, D., Córdón, A.M., Inventors, 2005, University of Cádiz, Spain. ES Patent 2221782 B1.
- Valdés-Solis, T., Marbán, G., Fuertes, A.B., 2001. Preparation of microporous carbon-ceramic cellular monoliths. *Microporous and Mesoporous Materials* 43, 113–126.
- Vergunst, T., Linders, M.J.G., Kapteijn, F., Moulijn, J.A., 2001. Carbon-based monolithic structures. *Catalysis Reviews* 43 (3), 291–314.
- Wang, C., Chang, K., Chung, T., 2004. Adsorption equilibria of aromatic compounds on activated carbon, silica gel and 13X zeolite. *Journal of Chemical Engineering Data* 49, 527–531.
- Yates, M., Blanco, J., Avila, P., Martín, M.P., 2000. Honeycomb monoliths of activated carbons for effluent gas purification. *Microporous and Mesoporous Materials* 37, 201–208.
- Zaitan, H., Chafik, T., 2005. FTIR determination of adsorption characteristics for volatile organic compounds removal on diatomite mineral compared to commercial silica. *Comptes Rendus Chimie* 8, 1701–1709.